Dynamics of (Micro)phase Separation during Fast, Bulk Copolymerization: Some Synchrotron SAXS Experiments

Anthony J. Ryan,† Wayne R. Willkomm,‡ Todd B. Bergstrom,§ and Christopher W. Macosko

Department of Chemical Engineering and Materials Science, University of Minnesota, Minneapolis, Minnesota 55455

Jeffrey T. Koberstein* and Chung Chien Yu

Institute of Materials Science and Department of Chemical Engineering, University of Connecticut, Storrs, Connecticut 06268

Thomas P. Russell

IBM Research Division, Almaden Research Center, San José, California 95120

Received June 25, 1990; Revised Manuscript Received December 14, 1990

ABSTRACT: The evolution of (micro)phase separation during the bulk formation of a copolyurethane has been followed by small-angle X-ray scattering (SAXS). The material examined comprised hard segments formed from 4,4′-diphenylmethane diisocyanate and 1,4-butanediol and soft segments based on a poly(oxyethylene-*block*-oxypropylene) diol of molar mass 2000. A small reaction injection molding machine was used to meter, mix, and inject stoichiometric amounts of reactants into a thermostated cell, fixed to an optical bench on beam line I–IV at the Stanford Synchrotron Research Laboratory. A full scattering pattern was collected every 0.7 s. Generally, higher polymerization temperatures led to a faster rate of (micro)phase separation but a lower ultimate degree of (micro)phase separation. An induction time was observed that decreased with increasing temperature. The scattered intensity at fixed angle increased with the square of time, and the length scale in the material increased with temperature. However, it was not possible to distinguish whether this structure was due to hard segment crystallization or noncrystalline microphase separation in this system.

Introduction

Reaction injection molding, RIM, is a method for the high-speed production of complex polymer parts directly from low-viscosity monomers or oligomers. The reactants are combined by high-pressure impingement mixing, and then they fill a mold, under low pressure, where they complete reaction to give a polymer part. The formation of solid polymeric material can involve cross-linking, (micro)phase separation, or crystallization or any combination of the three phenomena. The entire process, from mold closing and injection to demolding, can take place in less than 30 seconds. An excellent book concerning the fundamental science and engineering that underpins RIM has recently been published by Macosko.[1]

RIM materials are generally segmented block copolymers, the most common being copolyurethane,[2,3] copoly(urethane–urea)s,[4–6] copolyureas,[7–9] and copoly(ether amide)s.[10,11] The unique combination of physical properties available from segmented block copolymers is related to their (micro)phase separation. Typically such a polymer could be formed from 4,4′-diphenylmethane diisocyanate, MDI, reacting with butane-1,4-diol, BDO, and a polyether diol (normally of 2000–4000 molar mass). A high molecular weight segmented block copolymer is only formed in the special case of complete reaction.[12] At low conversions, the copolyurethane-forming system is generally a mixture of monomers and short hard segment sequences. At higher conversions, the material will be a mixture of unreacted polyether, short hard segment sequences, and di-, tri-, ..., multiblock copolymers; both the hard segment sequence length and the global molecular weight follow a most probable distribution if the reactants have functional groups of equal reactivity and the polymerization is homogeneous. The product from a typical RIM polymerization is thus a complex mixture of molecular species as depicted schematically in Figure 1.

The development of morphology during RIM polymerization is equally complex. As the chemical reactions proceed, the chain lengths (i.e., the average polymerization index, N) of all product species can increase. The interaction parameters (i.e., an average χ) can also change as a result of the accompanying chemical modifications. These collective changes may cause the system to cross thermodynamic phase boundaries. In the specific case of block copolymer species, an increase in the product χN can result in a thermodynamic transition from an initial homogeneous disordered state into an ordered (i.e., microphase-separated) state.[13,14] Homopolymer or oligomeric species can undergo a similar phenomenon, resulting in macrophase separation. Finally, crystallization of specific constituents may occur during this structural evolution. The resultant morphology may reflect all three of these phenomena and is determined in part by the kinetic competition between these processes.

RIM copolyurethanes have been extensively investigated by Macosko and co-workers;[1–3] for linear model materials, the factors determining final properties are hard segment content and crystallinity, the degree of (micro)phase separation, and copolymer molar mass. The dynamics of phase separation during fast, isothermal RIM copolyurethane polymerization have been investigated by Yang and

* Author to whom correspondence should be addressed.
† Current address: Manchester Materials Science Centre, University of Manchester Institute of Science and Technology, Grosvenor Street, Manchester M1 7HS, U.K.
‡ Current address: Dow Chemical Company, Texas Division, Building B1470D, Freeport, TX 77541.
§ Current address: Materials Science Department, Northwestern University, Evanston, IL 60208.

0024-9297/91/2224-2883$02.50/0

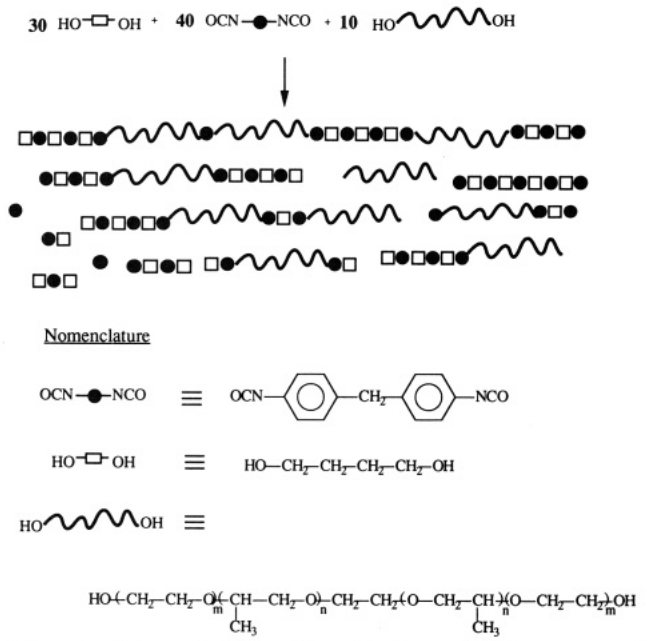

Figure 1. Schematic illustration of the formation of a segmented copolyurethane from a polyether diol and butane-1,4-diol reacting with 4,4′-diphenylmethane diisocyanate.

Macosko[3,15] for a range of catalyst contents and temperatures. A small RIM machine was used to inject impingement-mixed chemicals into either an FTIR spectrophotometer cell or between the plates of a parallel plate rheometer. The IR experiment was used to measure reaction conversion (through the isocyanate IR absorbance band) as well as phase separation dynamics (through the inter-urethane hydrogen-bonding behavior of the carbonyl IR absorbance bands). The onset of phase separation, indicated by the growth of the dynamic mechanical modulus, was found to be consistent with the IR behavior. These methods probe different length scales and different attributes of structural evolution, however, and therefore were found to give estimates of characteristic phase separation times that were not in agreement.

A well-characterized series of copolyurethanes have been studied by Koberstein and co-workers.[16-20] The thermal properties of these materials (i.e., hard segment melting point) depend strongly on their processing temperature.[17] Simultaneous FTIR/DSC[18] and synchrotron SAXS/DSC[19,20] experiments have been successful in elucidating the origins of this behavior. In particular, real-time synchrotron SAXS[19] and WAXD[20] measurements of the kinetics of microphase separation and crystallization showed that the competition between these two processes determined the final morphology.

In the present work, we apply the synchrotron SAXS technique to investigate the real-time structural evolution during the rapid, bulk (i.e., RIM) copolymerization of a polyurethane. In commercial RIM systems, polymerization and structure development are essentially completed in a time scale of seconds. For example, one of the most commercially interesting phase-separating copolymerizations (polyurea RIM) is complete in ~2 s and proceeds from a liquid with a viscosity of ~1 Pa s to a solid with a modulus of ~1 GPa in this time frame. It is quite remarkable that high molecular weight, well-structured materials can actually be prepared by this process.

This paper describes a real-time synchrotron SAXS study of phase separation during the bulk copolymerization of a polyurethane system based on MDI/BDO and a 2000 Dalton polyether diol. SAXS measurements were made at four different cell (mold) temperatures with all other processing parameters being held constant. These are our first efforts in trying to understand the complex ensemble of competitive structuring phenomena involved in RIM.

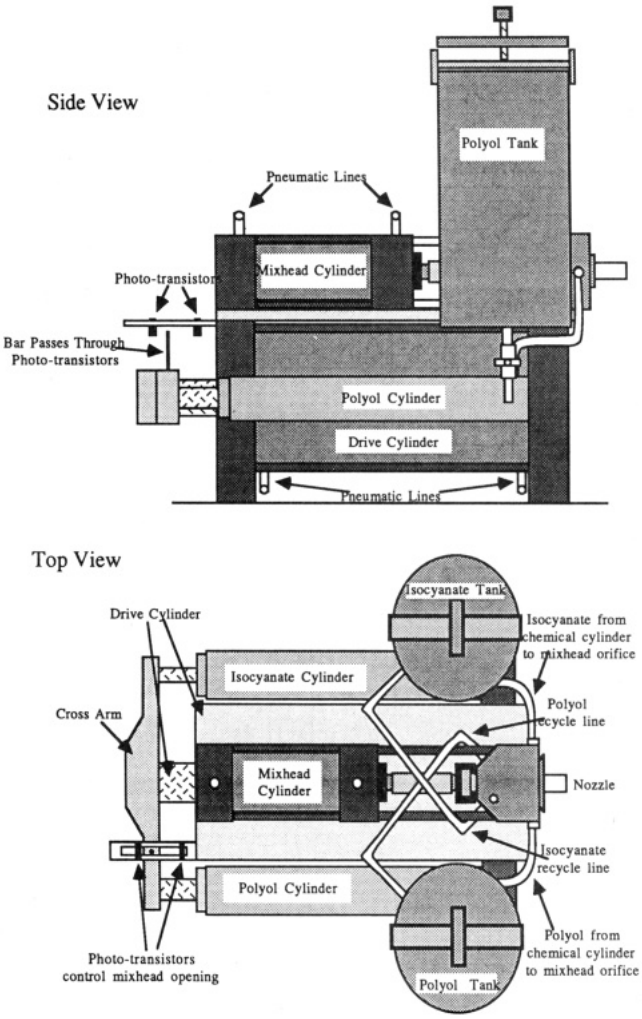

Figure 2. Schematic diagram of the micro-RIM machine (taken from ref 3).

Experimental Section

Materials. A three-component copolyurethane comprising pure 4,4′-diphenylmethane diisocyanate (MDI, Dow Chemical), butane-1,4-diol (BDO, Aldrich), and a poly(oxyethylene) end-capped (15% by weight) poly(oxypropylene) diol (M_n = 2000 Dalton, V5287, Dow Chemical) at 48% hard segment (weight fraction of MDI and BDO) was used throughout the study with a constant catalyst (dibutyltin dilaurate) content of 0.02% by weight. This system is virtually identical with that studied by Yang and Macosko[3,15] and similar in composition to the polyurethanes employed in the investigations of Koberstien and co-workers.[16-20]

Micro-RIM Machine. The Micro-RIM machine is designed to be portable to interface with analytical instruments.[21] A schematic diagram is shown in Figure 2. The mixhead is of the Macosko–McIntyre type with cross-flow recycle.[1,22] The stoichiometric ratio of reactants is controlled by the diameters of reactant cylinders and a fixed cross arm. The ratio is not continuously variable but is changed in steps by the diameter of the reactant cylinders. In this study, the volumetric flow rate was maintained at 2.05:1. The two chemical cylinders are driven pneumatically at a controllable rate to achieve good impingement mixing. The Reynolds number at the mixhead is typically above 500, which is greater than the critical Reynolds number required for turbulent flow through an orifice.[1] Temperature control of reactants is maintained by heating tapes wrapped around

Table I
Size Exclusion Chromatography Data (Polystyrene Standard) for the Materials Taken from the SAXS Cell

sample	$M_n/10^3$	$M_w/10^3$	M_w/M_n	T_{cell}/°C
PU1	10.5	64.2	6.1	60
PU2	9.2	51.0	5.5	70
PU3	13.5	68.5	5.1	102
PU4	13.9	93.2	6.7	118

the storage tanks and lines; reactant temperatures were maintained at 60 °C. A Macintosh II microcomputer and a Strawberry Tree Workbench A/D system were used to control the movement of mixhead in order to achieve a reproducible shot volume. A control menu and the shot time can be displayed directly on the screen of the Macintosh. The system is also equipped with a temperature and pressure collection package so that the process variables may be monitored.

SAXS Cell. A small volume, isothermal mold equipped with X-ray transparent polyimide windows was constructed from aluminum. It comprises two aluminum plates with countersunk holes of 3-mm diameter, two polyimide sheets, and an aluminum insert (2 mm thick) that is of a cross-sectional area 12 times that of the runner and gate assembly. The high viscosity and low flow rate provide for laminar material flow in the region of the windows. The cell could be placed reproducibly into a heating block and was mounted vertically on an X–Y translator for alignment with the X-ray beam. The mixed reactant stream was fed to the scattering cell through a 60-cm heated stainless steel tube (2-mm internal diameter) attached via a sized nozzle to the mixhead, giving material at the windows that is ~0.2 s old. The windows are disposable, and the mold insert could be cleaned and reused. The temperature inside the cell was measured by a thermocouple connected to the SAXS data accquisition system.

Synchrotron SAXS. The cell contains a 3-mm hole through which the focused X-ray beam can pass unhindered and is mounted in the SAXS apparatus of beam line I–IV at the Stanford Synchrotron Research Laboratory. The white light emanating from the synchrotron storage ring is focused by means of a float glass mirror and a bent, asymmetrically cut, Si(111) crystal. The Si monochromator is adjusted to deliver X-rays with a wavelength, λ, of 0.1429 nm. The incident-beam profile is defined with a number of antiscatter slits to give a cross section of approximately 1 mm² at the sample position. Scintillation detectors placed before and after the sample cell record the incident and transmitted intensities by diffraction from 10-μm-thick polyimide windows inclined at 45° with respect to the incident radiation; thus, changes in the specimen's attenuation factor are monitored continuously. The detector is a 1024-pixel EG&G Reticon photodiode array cooled to ca. -80 °C and placed several centimeters behind the focal spot of the X-rays. The detector assembly is interfaced with a DEC 11/34 computer via CAMAC electronics. The photodiode array is scanned every 25.6 ms, and at least 30 signals must be averaged before an output file containing the raw scattering profile can be written to disk. The experimental setup has been described previously.[23]

Size Exclusion Chromatography. Molecular weights and distributions were obtained by injecting a dilute 1-methyl-2-pyrrolidinone solution (0.1–0.2% polymer) into a stream of 1-methyl-2-pyrrolidinone (0.5 cm³/min) at 85 °C which passed through two 10-μm, mixed bed, cross-linked polystyrene columns on a Waters Model 150-C ALC/GPC equipped with a refractive index detector. Reported molecular weights are based upon a polystyrene calibration.

Results and Discussion

Real-time SAXS data were collected during polymerization at four temperatures (60, 70, 102, and 118 °C). Samples of polymer were removed from the cell and dissolved in 1-methyl-2-pyrrolidinone for size exclusion chromatography, and the molecular weight data are presented in Table I. The materials produced have high molecular weight with reasonable molecular weight distributions. For example, the values of M_n and M_w are higher than those for 50% hard segment RIM polyureas

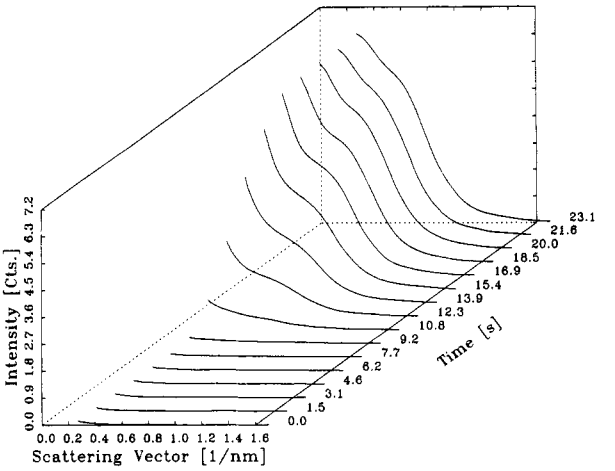

Figure 3. Evolution of small-angle scattering during a RIM polymerization at a cell temperature of 60 °C. Intensity, $I(\mathbf{q},t)$, versus scattering vector, $\mathbf{q}$, versus time, t.

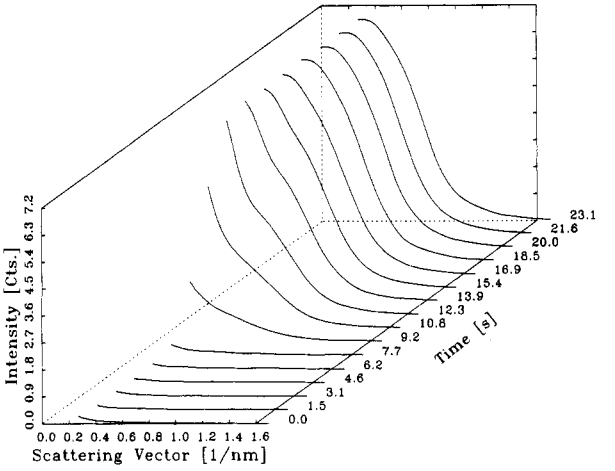

Figure 4. Evolution of small-angle scattering during a RIM polymerization at a cell temperature of 70 °C. Intensity, $I(\mathbf{q},t)$, versus scattering vector, $\mathbf{q}$, versus time, t.

reported by Willkomm et al.[8] The molecular weight distribution ($M_n/M_w \sim 6$) is somewhat broader than their value and could indicate that phase separation causes local stoichiometric imbalances which lead to compositional heterogeneities. MDI/BDO based polyurethanes formed under similar processing conditions by Camargo et al.[2] had M_w between 50 and 95 × 10³ and polydispersities of ~3. Virtually identical RIM polyurethanes have been reported by Yang[15] to have M_w between 32 and 92 × 10³ and polydispersities of ~2 depending on the temperature and catalyst content. The polydispersity of a polymer with the most probable distribution is 2. However, the experimental values reported have been derived from a polystyrene calibration and the overestimation of M_w and thus M_w/M_n by this procedure is well established.[24] The high molecular weights obtained indicate that initially the material was well mixed, whereas the breadth of the molecular weight distribution indicates that there were heterogeneities in the polymerizing mixture at some point.

The SAXS data for the four reaction temperatures are shown in Figures 3–6 as three-dimensional plots of intensity, $I(\mathbf{q},t)$, versus scattering vector, $\mathbf{q} = (4\pi/\lambda) \sin \theta/2$, where θ is the scattering angle, versus time, t. Qualitatively the curves show very little initial scattering, regardless of the cell temperature. This result indicates that the materials, upon injection into the cell, are either well mixed on the scale of several nanometers or demixed on a scale of several hundred nanometers. Combined with

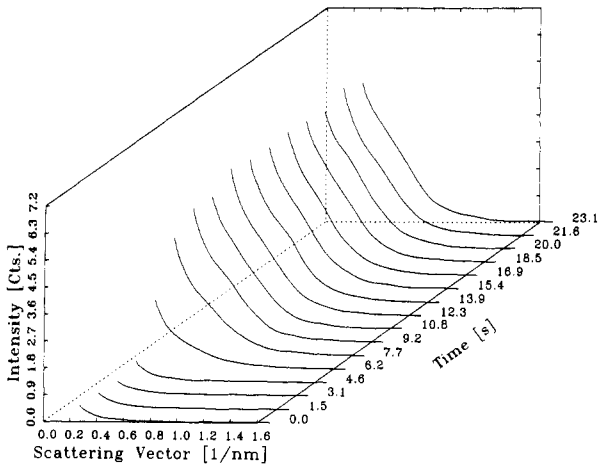

Figure 5. Evolution of small-angle scattering during a RIM polymerization at a cell temperature of 102 °C. Intensity, $I(\mathbf{q},t)$, versus scattering vector, $\mathbf{q}$, versus time, t.

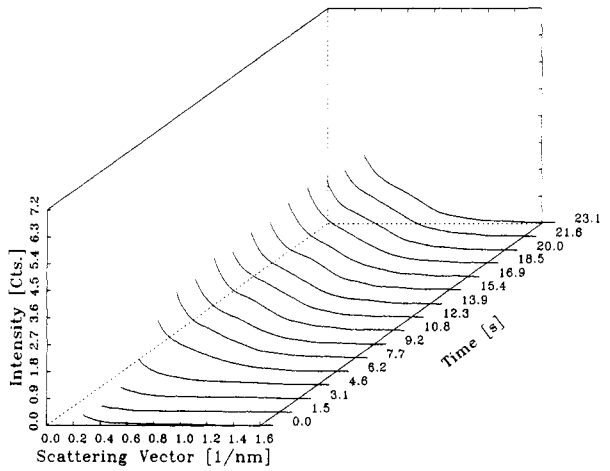

Figure 6. Evolution of small-angle scattering during a RIM polymerization at a cell temperature of 118 °C. Intensity, $I(\mathbf{q},t)$, versus scattering vector, $\mathbf{q}$, versus time, t.

the size exclusion chromatography data which indicated the formation of high polymer, these data show that the reactants were initially well mixed on a molecular level.

After an incubation period wherein significant scattering is absent, the scattered intensity in the small angle region develops gradually on a length scale of several hundred angstroms. The incubation period for structural development is inversely dependent on the cell temperature and is not discernible at 118 °C. The incubation period presumably corresponds to that portion of the polymerization process during which chain extension is occurring but that the chain length has not grown long enough to either crystallize or to exceed the critical lengths for either microphase or macrophase separation. Kinetic data[15] show that the rate of reaction and consequently the buildup of molecular weight are more rapid at higher temperatures, consistent with the decrease in incubation time as temperature is increased.

As the polymerization progresses, some of the SAXS data exhibit a shoulder in the scattering profiles that can be attributed to the formation of an ordered microphase structure (e.g., lamella θ). A monotonically decaying profile, in contrast, implies either a random microphase structure or an ordered microphase with dimensions too large to be resolved experimentally. The position of the shoulder ($\mathbf{q} \sim 1$ nm^{-1}) is consistent with a structure of the order of the radius of gyration of the soft segment oligomer,[8] as might be expected for an ordered polyurethane

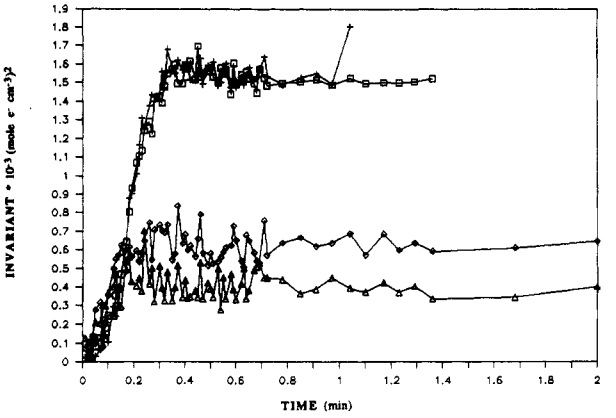

Figure 7. SAXS invariant, Q, as a function of time at 60 (□), 70 (+), 102 (◇), and 118 °C (△).

microdomain structure.[16,17]

The growth of intensity during polymerization can be related to the degree of microphase separation through calculation of the electron density variance. The ideal electron density variance of a perfectly separated two-phase system with sharp phase boundaries is defined by

$$\langle \eta_0^2 \rangle = \phi_1^0(\rho - \rho_1^0)^2 + \phi_2(\rho - \rho_2^0)^2 \quad (1)$$

where ρ is the material's average electron density and ϕ^0 and ρ^0 are the volume fractions and electron densities of the two pure phases, respectively. This value represents the maximum degree of microphase separation. The electron density variance of a real system will be lower than this value, since microphase separation is incomplete. In this case, the actual electron densities of each phase (ρ_1 and ρ_2) are closer to the average, leading to a decrease in electron density variance of the real system defined by

$$\langle \eta^2 \rangle = \phi_1(\rho - \rho_1)^2 + \phi_2(\rho - \rho_2)^2 \quad (2)$$

The value of $\langle \eta^2 \rangle$ will thus range from zero for a homogeneous mixture to $\langle \eta_0^2 \rangle$ for a fully microphase-separated block copolymer and is useful as an indication of the degree of microphase separation. Experimentally, the electron density variance may be calculated from

$$\langle \eta^2 \rangle = \frac{Q}{2\pi i_e} = \frac{1}{2\pi i_e}\int_0^\infty I(\mathbf{q})\,\mathbf{q}^2\,d\mathbf{q} \quad (3)$$

where i_e is the Thomposon scattering factor and the quantity Q is known as the invariant (being independent of the size or shape of the structural heterogeneities).

The experimental invariant can, therefore, be used to characterize the kinetics of structural development as well as the ultimate degree of microphase separation attained as a function of the RIM polymerization conditions. Invariant data at the four different cell temperatures are shown in Figure 7. At 60 and 70 °C, the incubation time of about 9 s is readily apparent and the phase separation process is essentially completed within 20 s. In contrast, the higher mold temperatures of 102 and 118 °C have no observable incubation time, with the phase separation process being completed within about 10 s. These data show quite clearly that the overall level of structure development during these bulk copolymerizations is inversely proportional to the polymerization temperature. The magnitude of the invariant at the lower temperatures of $\sim 1.5 \times 10^{-3}$ (mol e$^-$ cm^{-3})^2 compares with that of 1.6×10^{-3} (mol e$^-$ cm^{-3})^2 reported[25] at 80 °C for a compression molded 50% hard segment polyurethane made from similar reactants, whereas the long-time values of the invariant of 0.5×10^{-3} and 0.7×10^{-3} (mol e$^-$ cm^{-3})^2 at 102

and 118 °C indicate much lower degrees of (micro)phase separation.

Yang and Macosko[3] have studied the evolution of (micro)phase separation during bulk copolymerization by FTIR and rheological techniques. They found that there is an induction period before the evolution of either detectable hydrogen bonding or a measurable modulus that decreased from 6 to 3 to 1 s as the temperature was increased from 75 to 100 to 140 °C. Our data are in qualitative agreement with these results. However, the quantitative details of the correlation are hidden by the fact that each technique is using different information to detect the onset of (micro)phase separation. We detect the appearance of structure with electron density differences whereas they regard the onset of phase separation as the point at which the amount of free carbonyls begins to decrease and the formation of hydrogen-bonded carbonyls accelerates. Furthermore, while Yang and Macosko present excellent data on the evolution of hydrogen bonding and modulus, their methods are not capable of discerning mechanistic details of the microphase separation process.

The thermodynamics of diblock copolymer systems are complex and beyond the scope of this article. However, a few major features of the mean-field theory according to Leibler[26] and its development into the fluctuation theory of Frederickson and Helfand[27] will be highlighted. Due to the competition between the enthalpy and entropy of (micro)mixing, like monomer units will begin to aggregate at some temperature to form equilibrium microstructures; the relevant parameters in the theories are f, the copolymer composition, and the product χN, where χ is the Flory–Huggins interaction parameter and N is the degree of polymerization. This weak first-order process is known as the order–disorder transition, ODT, or the microphase separation transition, MST. The ordered, equilibrium, mesophase structures formed are predicted to be either a body-centered cubic array of spheres in a matrix or hexagonal close-packed rods or alternating lamella. These structures are composition dependent and have been observed experimentally for diblock and triblocks by a number of workers.[28,29]

The microphase separation transition for multiblock polymers is considered in the general theory presented by Hadziioannou and Benoit.[30] However, there are no predictions available for the kind of mesophase geometry expected, especially in the case of crystallizable segmented copolymers such as polyurethanes. Morphologies similar to those found in diblock copolymers have been reported in several microscopy investigations of polyurethanes.[31-33] Generally, the inherent polydispersity of segmented block copolymers leads to imperfect, nonequilibrium morphologies, which may be perfected upon annealing or other appropriate thermal cycling.[18,25,33]

The ultimate properties of RIM materials are drastically affected by their molecular weight and morphology. During RIM polymerization, several processes may occur that can influence the resultant molecular weight and morphology of polyurethanes. First of all, macrophase separation can take place between extended hard segment and soft segment species. Depending on the route the copolymerizing mixture takes through phase space, two distinct mechanisms may be observed,[34,35] namely, nucleation and growth (N&G) or spinodal decomposition (SD). In both cases for this process, macrophase separation proceeds until one phase vitrifies and/or crystallizes; the SD mechanism can lead to the formation of nonequilibrium morphologies, which comprise two interpenetrating networks, whereas the N&G mechanism leads to continuous-phase/discontinuous-phase morphologies.[35] Macrophase separation of this nature can limit molecular weight buildup by separating reactive groups. Further reaction is restricted to interfacial reaction to form block copolymer structures. Spinodal decomposition has a definite scattering signature: Cahn's linearized theory[36] predicts that the composition gradients, and thus scattered intensity, have a maximum for a given wavenumber and that in the early stages of the decomposition there is an exponential increase in the scattered intensity with time. This is obviously not the case in these systems (see Figures 3–6). The nucleation and growth process is not very well defined in terms of a kinetic scattering theory. However, the scattered intensity should fall monotonically with scattering vector and $I(\mathbf{q})$ has been observed to depend on time squared for well-characterized N&G systems.[37] We will return to this phenomenon later.

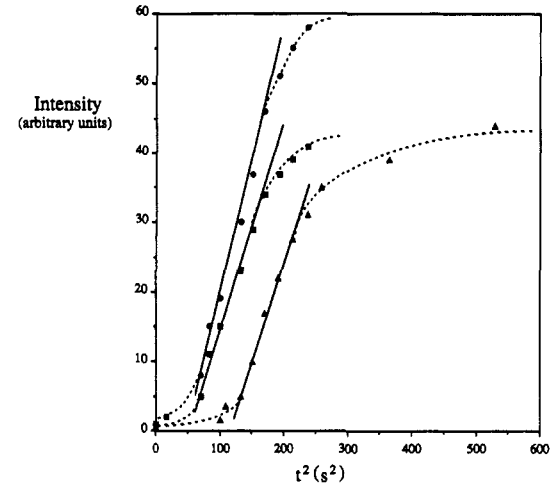

Figure 8. Intensity, $I(\mathbf{q})$, versus the square of time, t^2, for $\mathbf{q} \sim 1.0$ nm^{-1} (●) and 1.4 nm^{-1} (■) at 70 °C and $\mathbf{q} \sim 1.0$ nm^{-1} (▲) at 60 °C.

A number of block copolymer species form during the polymerization, first diblock species and then multiblock species, as chain extension continues. These species can undergo microphase separation as the molecular weight exceeds a critical value. This process can occur concurrently with macrophase separation. Block copolymer theory[26] predicts that the scattered intensity will diverge at a wave vector related to the dominant wavelength in the melt. However, the scattering pattern associated with the MST depends on the morphology formed and due to its long-range order may show higher order peaks.

Finally, microphase-separated and macrophase-separated hard segments may crystallize. The process of crystallization will show similar SAXS characteristics to both the N&G process of a mixture ($I(\mathbf{q}) \sim t^2$) and the microphase separation transition. (Bates et al.[38] have recently shown the kinetics of the disorder–order transition to be governed by secondary nucleation.)

Figure 8 shows the representative $I(\mathbf{q})$ versus t^2 curves, which show a good degree of linearity, a signature typical of a nucleation and growth process. We performed some visible light scattering studies in an attempt to resolve whether this process is microphase separation or crystallization. An experiment to measure the evolution of birefringence during polymerization proved unsuccessful as the polymerizing material was opaque on entering the cell. The use of shorter path lengths to circumvent this problem was precluded by the results of previous studies that demonstrated that the morphology of specimens formed

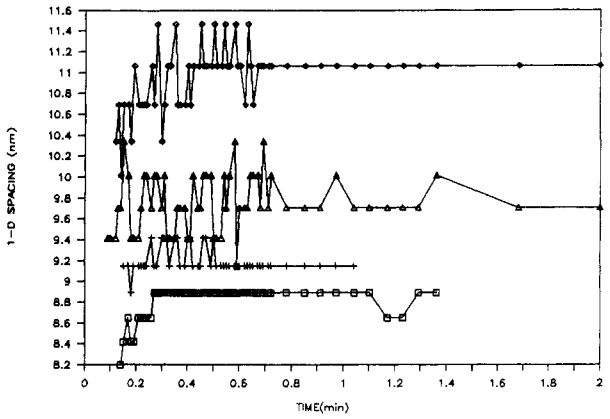

Figure 9. SAXS long period, 1-D, as a function of time at 60 (□), 70 (+), 102 (◇), and 118 °C (△).

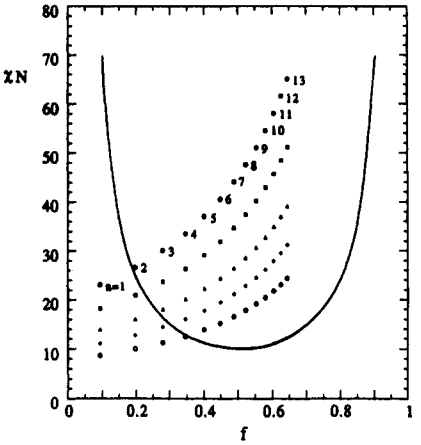

Figure 10. Location in phase space of hypothetical urethane diblocks containing n MDI residues at 25° (●), 50 (□), 75 (△), 100 (◇), and 125 °C (○). The value of χ was calculated using solubility parameters at 25 °C and estimated for the higher temperatures, N is the degree of polymerization normalized to poly(oxypropylene), and 1-f is the volume fraction of polyether. The solid curve is Leibler's microphase separation transition, MST, for diblock copolymers.[26]

in very thin sections (~micrometers) was different from that of specimens formed in relatively thick sections.

There are three pieces of experimental data that allow us to get closer to the fundamental structuring phenomena occurring in this bulk copolymerization. Firstly, there is a shoulder in the SAXS curves at $d \sim 6.3$ nm that is seen early in the structuring process. This is approximately twice the radius of gyration of the soft segment oligomer (3.4 nm according to Willkomm et al.[8]) and is where one would expect to see evidence of block copolymer lamellae. Secondly, shortly (less than a second) after the onset of (micro)phase separation, the material becomes opaque, indicating multiple scattering from structures on the order of the wavelength of visible light, while at the same time SAXS data show the persistent development of structure with a size scale of ~10 nm. This is inconsistent unless we have morphology consisting of a crystalline hard segment superstructure in a microphase-separated, segmented block copolymer matrix. Thus, SAXS probes the lamellar structure of the material while our eyes observe the semicrystalline superstructure. Thirdly, we form relatively high molecular weight material. This indicates that we did not have early nucleation and growth of a macrophase separating mixture and that the material, most probably, structures by competition between microphase separation and crystallization. Time-resolved wide-angle X-ray diffraction experiments have been used to study the evolution of structure in preformed polyurethanes[19] and are required in future work to distinguish between the processes of microphase separation and crystallization.

In an attempt to obtain some information regarding the periodicity of the microstructure formed, we assume that the material has a globally isotropic, locally lamellar morphology and obtain a one-dimensional Bragg spacing, d (1-D in Figure 9). This is done by applying the Lorentz correction, $\mathbf{q}^2$, to the observed scattered intensity and taking the maximum of the $I(\mathbf{q})\mathbf{q}^2$ versus $\mathbf{q}$ plot in the calculation of d.

$$d = \lambda/2 \sin \theta_{max} = 2\pi/\mathbf{q}_{max} \quad (4)$$

The evolution of d spacing with time is shown in Figure 9. There appears to be a growth in d in the early stages of the polymerization but these data are close to the resolution limit of the system. The asymptotic value of the d spacing is constant within the resolution of the instrument and increases with increasing temperature for the series 60 → 70 → 100 °C. These d spacings, between 9 and 12 nm, are small when compared to that of ~16 nm reported for the compression molded 50% hard segment polyurethane mentioned previously.[25] The persistence of the d spacing during the ordering process does not distinguish between possible ordering processes. Russell and Koberstein[39] found that the d spacing remained constant during the crystallization of polyethylene from the melt, and Hashimoto[40] observed the d spacing to remain constant during the ordering of block copolymers.

Koberstein and Stein[16] proposed a morphological model for polyurethanes that is based upon partial miscibility of hard segments with the soft phase according to their length. That is, there is a critical hard segment sequence length below which hard segments will be dissolved in the soft phase. Longer hard segments will segregate into a microdomain structure and may also crystallize. The hard segment domains are assumed to be lamellar, with a thickness that is proportional to the critical hard segment sequence length. As the temperature is increased, this critical length is expected to increase (assuming upper critical solution behavior). This model would thus predict an increase in the interdomain spacing, d, with an increase in temperature, consistent with our results. The partial dissolution process can be illustrated by considering the polyurethane to be equivalent to a polydisperse mixture of diblock polymers with constant soft block molecular weight (i.e., 2000) and a hard segment molecular weight that follows the most probable distribution. The various polyurethane copolymer species (depicted at five temperatures) will fall on phase space as shown schematically in Figure 10, where the solid curve is the MST for diblock copolymers.[26] The numbers on the figure denote the number of diisocyanate residues in the hard segment of each hypothetical diblock copolymer. The χ values used for these estimates were calculated from the solubility parameters, δ, at 25 °C.[40] Calculations at other temperatures are based on the assumption that both χ and δ are inversely dependent on temperature. The polyurethane diblock estimates for a particular temperature will intersect the MST curve at a particular number, which is indicative of the critical hard segment sequence length. This analysis suggests that at 25 °C (filled circles) hard segments with one diisocyanate residue will not segregate and thus will remain disordered (i.e., dissolved) within the soft microphase. As the temperature is increased (open symbols), the critical length obviously increases according to this scheme. The average molecular weight of the segregated or ordered hard segments would also subsequently increase as would the associated lamellar thickness and d spacing

(assuming that d is proportional to some power of the molecular weight, e.g., the $^2/_3$ power for well-segregated, normal diblocks[41]). The increase in critical length upon raising the temperature must necessarily be accompanied by additional intersegmental mixing, and this is consistent with the previously observed decrease in the invariant at higher temperatures. The partial miscibility model of Koberstein and Stein,[15] therefore, accounts qualitatively for both the experimental invariant and d-spacing data for bulk copolymerization to form a polyurethane.

Summary and Conclusions

We report the first time-resolved synchrotron small-angle X-ray scattering of structure formation and evolution during fast RIM polymerization of polyurethanes. The overall process comprises an induction period with little or no development of scattered intensity, followed by a period of rapid structural ordering. The induction period seems to involve chain extension up to a point at which the chain length is sufficient to either macrophase demix, microphase separate, or crystallize. After this point, the scattered intensity grows as the square of time, behavior consistent with nucleation and growth mechanisms of phase decomposition. As the temperature increases, the ultimate degree of microphase separation decreases and the interdomain spacing increases. This is consistent with the partial miscibility model for polyurethanes proposed by Koberstein and Stein, previous infrared spectroscopy results, and dynamic mechanical investigations of RIM polymerization. The results of this study, however, cannot distinguish whether the ultimate morphology is dominated by noncrystalline microphase separation, crystallization, or macrophase separation during polymerization. Future time-resolved X-ray diffraction experiments are planned to resolve the operant and dominant phase decomposition mechanisms in the overall RIM process.

Acknowledgment. We acknowledge the kind donation of the chemical reactants by the Dow Chemical Company. This research has been funded by the University of Minnesota's NSF Center for Interfacial Engineering (T.B.B.), National Science Foundation Grant NSF/CBT 8512120 (W.R.W., C.W.M.), a NATO Fellowship (A.I.R.), and the Office of Naval Research (J.T.K., C.C.Y.). Some of the materials incorporated in this work were developed at the Stanford Synchrotron Radiation Laboratory with the financial support of the National Science Foundation (DMR-77-27489) in cooperation with the Department of Energy.

References and Notes

(1) Macosko, C. W. *RIM Fundamentals*; Oxford University Press: New York, 1989.
(2) Camargo, R. E.; Macosko, C. W.; Tirrell, M.; Wellinghof, S. T. *Polymer* **1985**, *26*, 1145.
(3) Yang, W. P.; Macosko, C. W. *Makromol. Chem., Makromol. Symp.* **1989**, *25*, 23.
(4) Turner, R. B. *Polym. Comp.* **1984**, *5*, 151.
(5) Nissen, D.; Markovs, R. A. *J. Elastomers Plast.* **1983**, *15*, 96.
(6) Ryan, A. J.; Stanford, J. L.; Still, R. H. In *Integration of Polymer Science and Technology-2*; Lemstra, P. J., Kleintjens, L. A., Eds.; Elsevier: London; 1988; p 515.
(7) Dominguez, R. J. G. *J. Cell. Plast.* **1984**, *20*, 433.
(8) Willkomm, W. R.; Chen, Z. S.; Macosko, C. W.; Gobran, D. A.; Thomas, E. L. *Polym. Eng. Sci.* **1988**, *28*, 888.
(9) Ryan, A. J.; Stanford, J. L.; Wilkinson, A. N. *Polym. Bull.* **1987**, *18*, 517.
(10) Gabbert, J. D.; Hedrick, R. M. *Polym. Proc. Eng.* **1986**, *4*, 359.
(11) van der Loos, J. L. M.; van Geneen, A. A. *ACS Symp. Ser.* **1985**, *270*, 181.
(12) Peebles, L. H., Jr. *Macromolecules* **1974**, *7*, 872; **1976**, *9*, 58.
(13) Ryan, A. J. *Polymer* **1990**, *31*, 707.
(14) Ryan, A. J.; Stanford, J. L.; Still, R. H. *Plast. Rubb. Proc. Appl.* **1990**, *13*, 99.
(15) Yang, Y. P. Ph.D.. Dissertation, University of Minnesota, 1988.
(16) Koberstein, J. T.; Stein, R. S. *J. Polym. Sci., Polym. Phys. Ed.* **1983**, *21*, 1439.
(17) Leung, L. M.; Koberstein, J. T. *J. Polym. Sci., Polym. Phys. Ed.* **1985**, *23*, 1883.
(18) Leung, L. M.; Koberstein, J. T. *Macromolecules* **1986**, *19*, 706.
(19) Koberstein, J. T.; Russell, T. P. *Macromolecules* **1986**, *19*, 714.
(20) Galambos, A. F.; Russell, T. P.; Koberstein, J. T. Proc. 18th NATAS Conf., Paper 35, San Diego, CA, 24–27 Sept, 1989.
(21) Lee, L. J.; Macosko, C. W. *SPE ANTEC Tech. Pap.* **1978**, *24*, 151. Mikkelson, K.; Macosko, C. W. *J. Cell. Plast.* **1989**, *21*, 29.
(22) Macosko, C. W.; McIntyre, D. B. U.S. Patent 4,473,531, 1984.
(23) Stephenson, G. B. *SSRL Rep.* **1982**, *82*, 5.
(24) Lee, D.-C.; Speckhard, T. A.; Sorenson, A. D.; Cooper, S. L. *Macromolecules* **1986**, *19*, 2383.
(25) Galambos, A. F. Ph.D. Thesis, Princeton University, Princeton, NJ, 1989.
(26) Leibler, L. *Macromolecules* **1980**, *13*, 1602.
(27) Frederickson, G. H.; Helfand, E. *J. Chem. Phys.* **1987**, *87*, 697.
(28) See for example: Folkes, M. J.; Keller, A. In *The Physics of Glassy Polymers*; Haward, R. N., Ed.; John Wiley and Sons: New York, 1973; pp 548–597.
(29) *Processing, Structure and Properties of Block Copolymers*; Folkes, M. J., Ed.; Elsevier: New York, 1985.
(30) Benoit, H.; Hadziioannou, G. *Macromolecules* **1988**, *21*, 1449.
(31) Chen-Tsai, C. H. Y.; Thomas, E. L.; MacKnight, W. J.; Schneider, N. S. *Polymer* **1986**, *27*, 659.
(32) Li, C.; Goodman, S. L.; Albrecht, R. M.; Cooper, S. L. *Macromolecules* **1988**, *21*, 2367.
(33) Goodman, S. L.; Li, C.; Cooper, S. L.; Albrecht, R. M. *Proc. 46th Ann. Meet. Electron Microscopy Society of America*; San Francisco Press Inc.: San Francisco, 1988; pp 936–7.
(34) Binder, K. *Colloid Polym. Sci.* **1987**, *265*, 273.
(35) Olabisi, O.; Robeson, L. M.; Shaw, M. T. *Polymer–Polymer Miscibility*; Academic Press: New York, 1979.
(36) Cahn, J. W.; Hilliard, J. E. *J. Chem. Phys.* **1958**, *28*, 258.
(37) Lipatov, Y. S.; Grigor'yeva, O. P.; Kovernick, G. P.; Shilov, V. V.; Sergryeva, L. M. *Makromol. Chem.* **1985**, *186*, 1401.
(38) Bates, F. S.; Rosedale, J. H.; Frederickson, G. H. *J. Chem. Phys.* **1990**, *92*, 6255.
(39) Russell, T. P.; Koberstein, J. T. *J. Polym. Sci., Polym. Phys. Ed.* **1985**, *23*, 1109.
(40) Hashimoto, T. In *Physical Optics of Dynamic Phenomena and Processes in Macromolecular Systems*; Sedlacek, B., Ed.; Walter de Gruyter & Co.: Berlin, FDR, 1985; p 233.
(41) Ryan, A. J.; Stanford, J. L.; Still, R. H. *Polym. Commun.* **1988**, *29*, 196.
(42) Helfand, E.; Waserman, Z. R. In *Developments in Block Copolymers-1*; Goodman, I., Ed.; Applied Science Publishers: London, 1982.

Registry No. (MDI)(BDO)(EO)(PO) (block copolymer), 111938-02-4.